

EXPLORING THE MORPHOLOGY AND ORIGINS OF THE 4C 38.41 JET

JUAN CARLOS ALGABA^{1,2,3}, BINDU RANI^{4†}, SANG-SUNG LEE^{3,5}, MOTOKI KINO^{6,7}, JONGHO PARK^{2,8}, JAE-YOUNG KIM⁹

¹Department of Physics, Faculty of Science, University of Malaya, 50603 Kuala Lumpur, Malaysia

²Department of Physics and Astronomy, Seoul National University, 1 Gwanak-ro, Gwanak-gu, Seoul 08826, Korea

³Korea Astronomy & Space Science Institute, 776, Daedeokdae-ro, Yuseong-gu, Daejeon, Republic of Korea 305-348

⁴NASA Goddard Space Flight Center, Greenbelt, MD 20771, USA

⁵Korea University of Science and Technology, 217 Gajeong-ro, Yuseong-gu, Daejeon 34113, Korea

⁶Kogakuin University of Technology & Engineering, Academic Support Center, 2665-1 Nakano, Hachioji, Tokyo 192-0015, Japan

⁷National Astronomical Observatory of Japan, 2-21-1 Osawa, Mitaka, Tokyo, 181-8588, Japan

⁸Academia Sinica, Institute of Astronomy and Astrophysics, P.O Box 23141, Taipei 10617, Taiwan

⁹Max-Planck-Institut für Radioastronomie, Auf dem Hügel 69, D-53121 Bonn, Germany

Accepted for publication in ApJ.

ABSTRACT

We study the properties of the innermost jet of the flat spectrum radio quasar 1633+382 (4C 38.41) based on VLBI data from the radio monitoring observations of the Boston University VLBI program at 43 GHz. Analysis of the components suggests a semi-parabolic jet geometry with jet radius R following the relation $R \propto r^{0.7}$ with distance r , with indications of a jet geometry break towards a conical geometry. Brightness temperature falls with distance following $T_B \propto r^{-2.1}$. Combining this information, magnetic field and electron densities are found to fall along the jet as $B \propto r^{-1.5}$ and $n \propto r^{-1.1}$ respectively, suggesting that the magnetic configuration in the jet may be dominated by the poloidal component. Our analysis of the jet structure suggests that the innermost jet regions do not follow a ballistic trajectory and, instead, match a sinusoidal morphology which could be due to jet precession from a helical pattern or Kelvin-Helmholtz instabilities.

Subject headings: galaxies: active — galaxies: jets — quasars: individual (4C 38.41)

1. INTRODUCTION

The source 1633+382 (4C 38.41) is a flat spectrum radio quasar (FSRQ) at a redshift $z = 1.813$ (Hewett & Wild 2010). Strong variability in its radio flux has been observed (Spangler & Cotton 1981; Kühn et al. 1981; Seielstad et al. 1985; Aller et al. 1992) and superluminal motion with jet velocities up to $394 \pm 23 \mu\text{as yr}^{-1}$ ($30.8 \pm 1.8 c$) has been detected (Lister et al. 2019). 4C 38.41 is also well known to be one of the most powerful γ -ray extragalactic objects (Abdo et al. 2009; Acero et al. 2015), with prominent γ -ray outbursts.

The γ -ray flares have been considered to be connected with interaction with emerging VLBI components (Jorstad et al. 2011) or with Doppler boosting variations geometrically connected to changes in the viewing angle (Raiteri et al. 2012). Algaba et al. (2018a) (hereafter, Paper I) found that major γ -ray flares were well matched with similar activity in optical and radio bands, with gamma-ray flares leading radio flares. Considering the shock-in-jet model, it was estimated that the location of the radio emitting regions was of the order of 40 pc from the central engine. Algaba et al. (2018b) (hereafter, Paper II) showed that several γ -ray flares coincided with the ejection of respective new very long baseline interferometry (VLBI) components which evolved with predominantly adiabatic losses. The source of activity was considered to be dominated with a particle-dominated region, possibly near but downstream the acceleration and collimation region.

Although the ejection of components has been extensively analysed, the overall structure of the jet is still not

very well studied. Very Large Array (VLA) observations have found that its kiloparsec scale morphology shows a core-dominated triple structure in the north-south direction with an extent of about 12 arcsec (Murphy et al. 1993), whereas parsec scales show a misalignment of about 90° with a single-jet structure detected by the Very Long Baseline Array (VLBA) toward the west. It has been estimated that the parsec-scale jet is aligned at $\sim 1^\circ - 3^\circ$ to our line of sight (Hovatta et al. 2009; Liu et al. 2010).

Several authors have recently studied the innermost structure of the jet. In Pushkarev et al. (2017) the regions within the upper 100 mas were fitted with a power law suggesting a conical jet with power index $\epsilon = 0.95 \pm 0.01$, whereas the 5 mas showed an almost parabolic jet with $\epsilon = 0.57 \pm 0.01$, where $\epsilon = 1$ for the purely conical and $\epsilon = 0.5$ for the purely parabolic cases. Nonetheless, no further discussion was conducted. On the other hand, Algaba et al. (2017) found a rather conical geometry with $\epsilon = 0.14 \pm 0.21$ for the innermost jet scales based on a fit of the core sizes considering core shift effect indicated, albeit subjected to sparse and possibly variable data. The evolution along the jet of the physical parameters, such as magnetic field strength or electron density are however not well studied.

In this paper we study the properties of the jet within the first milliarc-seconds from the VLBI core region. In particular, we examine the flux density, brightness temperature and collimation profile. Based on our findings, we additionally investigate the magnetic and electron density profiles, the physical origin of the jet in this source, and possible implications. The contents of the paper is organized as follows: In Section 2, we summa-

[†]NASA Postdoctoral Program (NPP) Fellow

alize the observations and data analysis. In Section 3 we compile our results. In Section 4 we discuss the implications of our results, and in Section 5 we draw our conclusions.

2. OBSERVATIONS AND DATA ANALYSIS

For our analysis, we considered the data from the Boston University (BU) 43 GHz Monitoring program¹. The model-fitted data from Jorstad et al. (2017) contains models for epochs spanning from 2007 June 15th to 2013 January 16th. To complement this data, we included the model-fitted data analysed in Paper II corresponding to observations during the period 2012 March – 2015 June. In Paper II we discussed the data processing, including components fitting. Here we briefly summarize the methodology. We used the Caltech *Difmap* package (Shepherd 1997) to model-fit the various components of the VLBA data. In addition to the core, we could fit other long-lived components that we identify as C2, C3 and C4. We considered resolution limits as given by Lobanov (2005) and filter out non-resolved components. If the component appears to be resolved, we consider their distance relative to the core position, and the uncertainty estimates are given for the size, distance, flux density and position angle as $\sigma_d \sim d/\sqrt{DR}$, $\sigma_r \sim (1/2)\sigma_d$, $\sigma_F \sim \sigma_{rms}\sqrt{DR}$ and $\sigma_{PA} \sim \arctan(\sigma_r/r)$ respectively, for dynamic ranges $DR \gg 1$ (see e.g. Fomalont et al. 1999; Lee et al 2008), where σ_{rms} is the map root mean square noise level. When combining the two data sets, we obtained a total of 88 unique epochs from 2007 June 15th to 2015 June 9th.

Due to the core shift effects, the location of the VLBI core does not correspond to that of the central engine. Thus, in order to properly measure the position of the components with respect to the central engine, we need to take this effect into account and consider which is the core shift of this source at 43 GHz. For this, we obtained the core shift measure and core shift at 15.4 GHz from Pushkarev et al. (2012) and estimated the core shift at 43 GHz to be $\Delta r = 14 \pm 4$ pc (see also Paper I). This corresponds to angular scales of $\Delta r = 0.06 \pm 0.02$ mas which, although quite small, are still significant for VLBA observations at 43 GHz, with beam sizes of the order of 0.2 mas, suggesting practical achievable resolutions of the order of 0.04 mas when considering high dynamic ranges (typically 400:1 or higher; see, e.g., Jorstad et al. 2017, Paper II) of the VLBA images (Lobanov 2005). Thus, even such small core shift is comparable with the scales measured here and will have practical effects in the proper analysis of the jet component positions when studied relative to the central engine. In the following we focus on the results considering the distances with respect to the central engine.

3. RESULTS

A dedicated study of components distance from the core, including calculations regarding ejection epoch and speed, was already shown in Paper II. Here we focus on other phenomenological characteristics of the components. In Figure 1 we show the trajectories of the jet components in the RA–DEC plane. The most remarkable feature is an apparent bending of the jet direction.

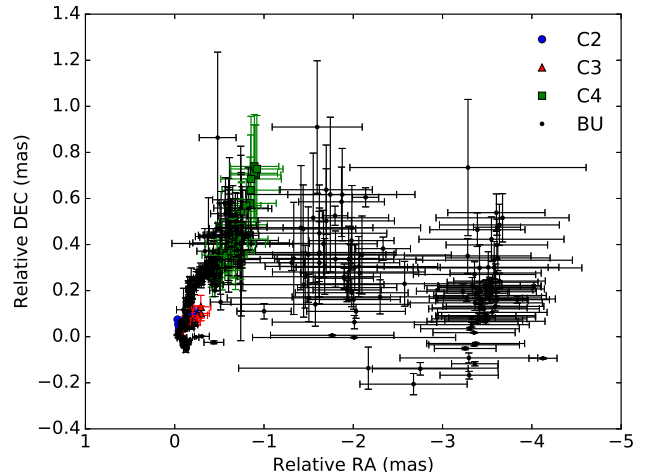


FIG. 1.— Trajectories of the jet components in the RA - DEC plane, where $RA = r \cos(\Theta + 90)$ and $DEC = r \sin(\Theta + 90)$. Here, r is the radial distance from the core, and Θ is the position angle of the component with respect to an imaginary north-south line drawn through the map center. Blue circles, red triangles, green squares and black dots indicate components C2, C3, C4 and these from BU Blazar program described in Jorstad et al. (2017), respectively.

Although the uncertainties are comparatively large at distances > 2 mas, it is clear that the jet direction does not remain constant and there is a significant bending at a distance of ~ 1 mas from the core. Indeed, the median value for the jet position angle for distances under ~ 1 mas is about $\langle PA \rangle \sim -59^\circ$, whereas for larger distances, $\langle PA \rangle \sim -85^\circ$.

Evolution of flux density with distance is shown in Figure 2. Flux density monotonically decreases with distance from the core, with the exception of a slightly larger flux observed in the furthest components (at ~ 3.5 mas from the core) of the BU data. A plateau in the flux density is also noticeable around ~ 0.4 mas, although several components appear to have a lower flux densities between 0.2-0.3 mas. It is possible that we are tracing the flux of various different components that intrinsically started with different flux density, leading to a fiducial flux density profile, and in particular, a plateau, along the jet. However, identification of C4 component with that labeled B1 in Jorstad et al. (2017) suggests otherwise, as this component seems to have always been below the 1 Jy threshold.

Figure 3 shows the deconvolved FWHM of components as a function of distance. The jet component size increases with distance from the core. If we interpret the FWHM of the components with the jet diameter, we can relate the FWHMs as a probe to estimate the jet radius R , which we consider to vary with distance r in the form $R \propto r^\epsilon$, with $\epsilon = 1$ for a purely conical and $\epsilon = 0.5$ for a pure parabolic case, respectively (Algaba et al. 2017). Due to the large scatter and uncertainties, we considered a Markov-chain Montecarlo (MCMC) method (Foreman-Mackey et al. 2013) to obtain a more robust fit to the data. A fit including all components indicates $\epsilon = 0.62 \pm 0.01$ considering distances from the VLBI core, or $\epsilon = 0.71 \pm 0.02$ if we consider core shift effects: i.e. from the central engine. This suggests that the jet components in this source follow a quasi-parabolic geometry

¹ <https://www.bu.edu/blazars/VLBAproject.html>

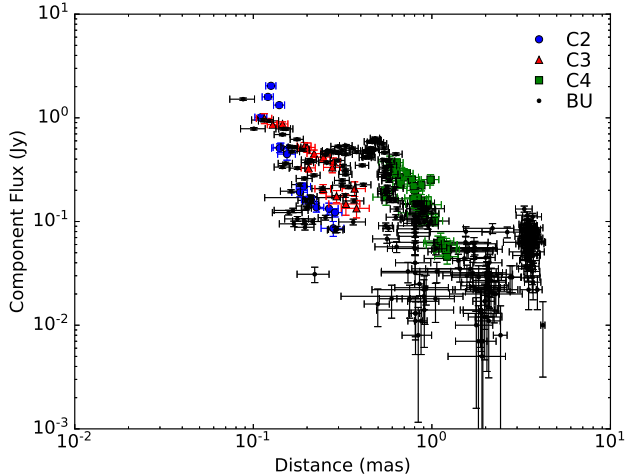


FIG. 2.— Components flux as a function of distance. Top: as observed, considering distances from the 43 GHz VLBI core. Bottom: considering distances from the central engine, including the core shift at 43 GHz. Color markers and shapes are as Fig. 1.

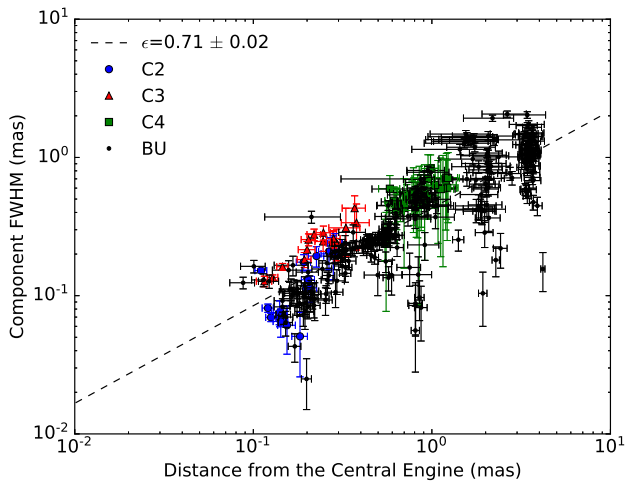


FIG. 3.— Components size as a function of distance. Markers color and shape, and top and bottom panels as in Figure 2.

at the distances probed here.

The redshift-corrected brightness temperature T_B of the bright emission features can be approximated using the following relation (Jorstad et al 2005):

$$T_B = 1.22 \times 10^{12} \frac{S_{comp}(1+z)}{FWHM^2 \nu^2} \text{ K}, \quad (1)$$

where S_{comp} is the component flux density in Jy, ν is the observing frequency in GHz, and the FWHM is measured in mas². Table 1 summarizes the derived components brightness temperature, and Figure 4 shows them as a function of distance from the core, together with the brightness temperatures from the BU data (Jorstad et al. 2017)

² Some authors (e.g. Kovalev et al 2005) include the factor $(1+z)$ in the numerator, while others (e.g. Hovatta et al. 2009) include it in the denominator. This will not affect our results since it will appear as a constant factor.

TABLE 1
BRIGHTNESS TEMPERATURES

Date (1)	MJD (2)	T_b ($\times 10^9$ K)		
		C2 (3)	C3 (4)	C4 (5)
2012 Apr 03	56021	—	19 ± 13	4.4 ± 1.6
2012 May 27	56074	—	—	3.2 ± 2.1
2012 Jul 05	56113	—	38 ± 22	4.1 ± 1.9
2012 Aug 13	56153	—	478 ± 130	3.1 ± 1.4
2012 Oct 07	56208	—	96 ± 30	2.5 ± 1.3
2012 Oct 19	56220	—	80 ± 22	2.4 ± 1.5
2012 Oct 27	56228	—	58 ± 18	2.6 ± 1.4
2012 Oct 28	56229	—	—	2.8 ± 1
2012 Dec 21	56283	—	116 ± 75	2.2 ± 2.8
2013 Jan 15	56308	—	87 ± 15	2.1 ± 0.7
2013 Feb 26	56350	—	62 ± 13	2 ± 0.7
2013 Apr 17	56399	—	30 ± 12	1.6 ± 1
2013 May 31	56443	—	31 ± 17	1.6 ± 1.3
2013 Jul 01	56474	65 ± 16	6 ± 3	1.2 ± 0.5
2013 Jul 29	56502	48 ± 14	—	1.5 ± 0.9
2013 Aug 26	56531	81 ± 24	5.6 ± 4	1.1 ± 0.8
2013 Nov 18	56615	447 ± 118	10.5 ± 6.1	1.2 ± 1
2013 Dec 16	56643	442 ± 67	8.1 ± 3.1	1 ± 0.6
2014 Jan 20	56678	780 ± 123	9.5 ± 3.3	0.7 ± 0.3
2014 Feb 25	56714	491 ± 82	10 ± 3.1	0.7 ± 0.3
2014 May 04	56781	227 ± 122	2.1 ± 1.8	0.5 ± 0.6
2014 Jun 21	56829	166 ± 90	2.2 ± 2.3	0.8 ± 0.9
2014 Jul 29	56867	222 ± 145	2.9 ± 3.3	1 ± 1.3
2014 Sep 23	56924	115 ± 54	—	1.3 ± 0.7
2014 Dec 05	56997	22 ± 8	—	1.2 ± 0.4
2015 Apr 12	57124	6 ± 4	—	1.2 ± 0.7
2015 May 12	57154	4 ± 4	—	1 ± 0.7
2015 Jun 09	57182	4 ± 2	—	1 ± 0.4

Brightness temperatures are of the order of 10^{11} K for the innermost components and, similar to the flux density, decrease with distance down to about 10^7 K in the further components presented here. Evolution of the brightness temperature seems to follow a pattern similar to that of the flux density, with indications of a possible plateau also at 0.3-0.4 mas. A fit of the brightness temperature of the various components as a function of distance in the form $T_B \propto r^{-f}$ indicate $f = 2.1 \pm 0.1$ and 2.3 ± 0.1 when we do not and we do consider the core shift, respectively.

4. DISCUSSION

4.1. Jet Geometry

In this paper we study the properties of the innermost regions of the 1633+382 jet. As we anticipated in Section 2, the 43 GHz VLBI core distance from the central engine is comparable to the scales of the closest components analyzed here, which implies that its consideration will have a significant impact in the interpretation of our results, as seen in Figures 2, 3, and 4. Given that we regard the location of the central engine as the upstream end of the jet derived from the core shift, we will hereafter concentrate our discussion based on analysis taking the core shift into account.

Our results above show that the jet width follows a semi-parabolic geometry, with $\epsilon \sim 0.7$, between the pure conical and the parabolic cases. Similar results are obtained using the data from Jorstad et al. (2017), which leads to $\epsilon = 0.66 \pm 0.02$ (Note that their published data

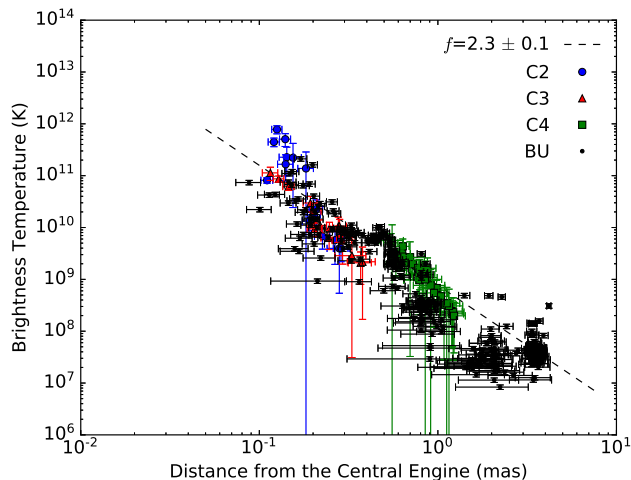


FIG. 4.— Components brightness temperature as a function of distance. Markers color and shape, and top and bottom panels as in Figure 2.

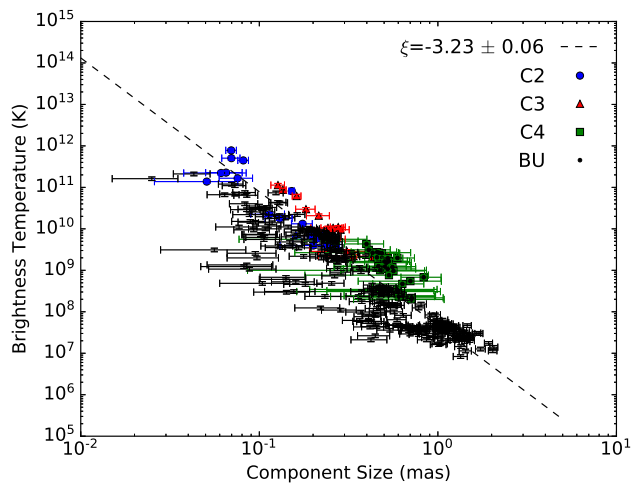


FIG. 5.— Components brightness temperature as a function of component size. Markers color and shape, and top and bottom panels as in Figure 2.

spans a different time range than the one discussed here). We find however a discrepancy with the results found in Algaba et al. (2017), where a study based on core sizes related with their respective core-shifted locations suggested a rather conical structure with $\epsilon = 1.14 \pm 0.21$ for this source. This value is clearly larger than the one found here. We note however that the results in Algaba et al. (2017) are susceptible to variability effects, as the data used there was not simultaneous. It may also be possible that these two methods are probing different jet regions of 1633+382, since the core size was used in Algaba et al. (2017), whereas we only include optically thin jet structure in this work. Another possibility is that we may be probing even different jet structure, if an unresolved spine–sheath morphology, such as the one seen in M87 (Asada et al 2016), is present in this source; or if, given the small viewing angle, we may be actually looking throughout the jet itself as we approach the regions near the base of the jet, thus affecting the observed geometry.

Semi-parabolic jet geometries have been conclusively found in other sources such as M87 (Asada & Nakamura 2012), NGC6251 (Tseng et al. 2016), NGC4261 (Nakahara et al. 2018) or 1H0323+342 (Hada et al. 2018). In these sources, this geometry is found upstream the jet, before a transition towards a conical geometry occurs at around the Bondi Radius, at about few $10^5 r_s$, where r_s is the Schwarzschild radius. For the case of 1633+382, the semi-parabolic geometry is found on scales of a milliarcsecond, which translate to projected distances of the order of $\lesssim 8.5$ pc; or $\lesssim 250$ pc deprojected, assuming a viewing angle of $\theta \sim 2^\circ$ to our line of sight (Hovatta et al. 2009; Liu et al. 2010). If we consider the central engine to host a supermassive black hole with a mass of $M \sim 1.32 \times 10^9 M_\odot$ (Zamaninasab et al. 2014), such distances are of the order of $\lesssim 2 \times 10^6 r_s$. This is slightly larger but of the same order of magnitude than the scales discussed in the literature for the other sources.

A more quantitative estimation of the regions being probed here can be done as follows. The Bondi radius can be obtained from $r_B = 2GM/c_s^2 = (c/c_s)^2 r_s$, where G is the gravitational constant and the sound speed $c_s = \sqrt{\gamma k_B T / (\mu m_p)}$ is a function of gas temperature T , $\mu (= 0.6)$ is the mean molecular weight, $\gamma (= 5/3)$ is the adiabatic index of the accreting gas, and m_p is the proton mass. Bednarek & Kirk (1995) estimated a maximum temperature of about 0.30 keV, which allows us to estimate $r_B \gtrsim 2 \times 10^6 r_s$. Alternatively, the sphere of gravitational influence (SGI), the radius inside of which the black hole gravitational potential dominates, can be written as $r_{SGI} = GM_{BH}/\sigma^2 = (1/2)(c/\sigma)^2 r_s$, where σ is the stellar velocity dispersion. Based on the M – σ relationship (see e.g. Gebhardt et al. 2000; Ferrarese & Merrit 2000; Merritt & Ferrarese 2001; McConnell et al. 2011), we can consider $M_{BH} = 1.9 \times 10^8 M_\odot (\sigma/[200 \text{ km/s}])^{5.12}$, and evaluate $\sigma \sim 290 \text{ km s}^{-1}$. With such velocity dispersion, we estimate $r_{SGI} \sim 5.5 \times 10^5 r_s$.

The estimated Bondi radius and the radius of gravitational influence appear to have a similar order of magnitude than that of the regions downstream the jet measured in our data. Although the uncertainties are very large, it is possible that our observations are probing the quasi-parabolic geometry of the regions where the gravitational potential of the black hole is still dominant with respect to the thermal energy of the hot gas in the environment, if the same phenomenology seen in M87 and NGC6251 also applies to 1633+382.

In order to investigate this more deeply, we consider the jet geometry in terms of gravitational radii $r_g = GM/c^2$. For 1633+382, $1 \text{ mas} \sim 4 \times 10^6 r_g$, considering deprojection effects. In Figure 6 we plot the jet geometry in terms of r_g adding the 43 GHz VLBA-BU Blazar Monitoring Program data as presented in Jorstad et al. (2017), the jet width as in Pushkarev et al. (2017), and the jet width from the 1.4 GHz VLBI observations from the University College Cork program³. We corrected for the core shift effects at each frequency considered. It seems apparent that the geometry of the jet falls well within the area delimited by the genuine parabolic and the conical streamlines (compare this with Figure 3 of

³ http://www.physics.ucc.ie/radiogroup/18-22cm_observations.html

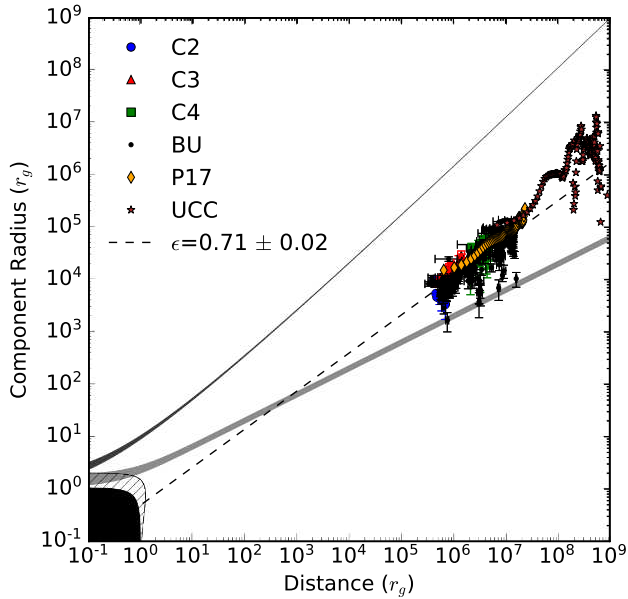


FIG. 6.— Jet radius of 1633+382 including the data from the components discussed here and the 43 GHz BU VLBA Blazar program data, in units of gravitational radii. Markers color and shape are as in Figure 2, with orange diamonds indicating the data from Pushkarev et al. (2017) and brown stars the data from the 1.4 GHz VLBA University College Cork Program. The filled black region denotes the black hole (inside the event horizon), while the hatched area represents the ergosphere for the black hole spin parameter $a=0.998$. Dashed line represents $R \propto r^{0.7}$. The light gray area denotes the genuine parabolic streamline ($R \propto r^{1/2}$ at $R \gg r_g$) of the force-free steady jet solution, while the dark gray area denotes the quasi-conical streamline ($R \propto r^{0.97}$ at $R \gg r_g$) of the force-free steady jet solution. In both streamlines, a variation from $a=0.5$ (upper boundary) to $a=0.998$ (lower boundary) is considered as a shaded area. Note that all streamlines are anchored at the event horizon in polar coordinates in the Boyer-Lindquist frame, which matches the data coordinates for $R \gg r_g$.

Algaba et al. (2017)).

While components upstream the jet appear to follow a quasi-parabolic geometry, data from Pushkarev et al. (2017) may not follow this extrapolation towards larger radii, and data from University College Cork shows a clear deviation, suggesting that such quasi-parabolic geometry may not be the case downstream, and a jet geometry break may occur near this region. However, when considering a smoothly connected broken power law to check this possibility, uncertainties were dramatically large and results were not reliable, possibly due to the significant oscillation in the jet radius from the University College Cork data. We note that this data correspond to a single epoch observation. Nonetheless, Pushkarev et al. (2017) fitted the whole region as a geometrically conical jet, with $\epsilon = 0.95 \pm 0.01$. This supports the possibility of a jet geometry break near the Bondi radius. This phenomenology has the features of the one seen in M87 (Asada & Nakamura 2012), NGC6251 (Tseng et al. 2016) or 3C 273 (Akiyama et al. 2018). If this is the case, this would strongly support a unification in the jet geometry aspects for various kinds of AGN.

The extrapolation of the jet width (dashed line in Figure 6) suggests that the jet foot point is located at a certain distance of the SMBH (for a jet radius = $1 r_s$,

the distance is $2.0 \pm 0.7 r_s$). If so, this may point towards a rotationally driven outflow (Blandford & Znajek 1977) mechanism for the jet origin. This scenario would give rise to a leptonic jet with little matter load, and initially Poynting flux dominated, in tension with the results from Paper II, which suggested a particle-dominated region for the new jet components ejection.

It is possible however that the trend analyzed here does not hold upstream the jet. On the other hand, as we mentioned above, our observations are reaching these regions where the jet opening angle is larger than the viewing angle and we are inspecting *through* the jet, which would affect our discussion. This effect may be even more significant if the jet consists of a spine and sheath, as mentioned above.

In order to check for this and the robustness of our results, the jet geometry needs to be scrutinized with data spanning more decades along the jet. Given that we need to probe towards the vicinity of the central engine, within the Bondi radius region, high resolution VLBI observations, with e.g., RadioAstron, the Event Horizon Telescope (EHT) (e.g., Doeleman et al. 2012; Lu et al. 2013; Gómez et al. 2016; EHT Collaboration et al. 2019) or future facilities and instruments such as Millimetron (Kardashev et al. 2014), will be necessary.

Based on a number of theoretical studies (see e.g., Komissarov et al 2007, 2009; Tchekhovskoy et al 2008; Lyubarsky 2009), we expect to observe deviations from equipartition at the jet base that should be dominated by the magnetic field. This energy should be converted to kinetic energy as the bulk acceleration proceeds; however, this is not observed in 1633+382, at least not on the scales examined on this study. Unlike M87, the source shows collimation but not acceleration. Other studies (e.g., Kino et al. 2002; Homan et al. 2006; Nokhrina 2017; Pilipenko et al. 2018) have also proposed models where the energy density of particles dominates over that of the magnetic field in the innermost regions, as appears to be the case for 1633+382. In order to investigate and understand this in more detail, sub-mm observations of this source will be useful.

4.2. Magnetic Field and Electron Densities

Under an assumption of a jet with constant Lorentz factor of the emitting electrons and power-law dependences of the particle density, magnetic field strength and jet transverse size in the form $N_e \propto r^{-n}$, $B \propto r^{-b}$, and $R \propto r^\epsilon$, the brightness temperature for optically thin synchrotron emission should follow a power law (Kadler et al 2004; Kravchenko et al. 2016; Beuchert et al. 2018)

$$T_{b,jet} \propto r^{-f} \quad ; \quad f = -\epsilon + n + b(1 - \alpha). \quad (2)$$

The parameter n can be constrained a priori by the geometry of the outflow, since $N_e \propto R^{-2}$. This does not require any assumption about the physical conditions in the jet and only requires mass conservation. If we take $\epsilon = 0.71 \pm 0.06$ and $f = 2.3 \pm 0.1$, we find $n = 1.4 \pm 0.1$. This leads to the relation $1.6 = b(1 - \alpha)$. For small values of the spectral index, this suggests $1 < b < 1.6$.

If we consider core shift effects, we can go a step further. In general, the position of the core is proportional to the frequency in the form $r_c(\nu) \propto \nu^{-1/k_r}$, where the coefficient k_r holds information about physical conditions

in the ultracompact jet region:

$$k_r = \frac{(3 - 2\alpha)b + 2n - 2}{5 - 2\alpha}. \quad (3)$$

In the same manner, under the assumption that each jet component is an independent relativistic shock with adiabatic losses dominating the emission, we can consider (Marscher 1990):

$$T_{b,jet} \propto d^\xi \quad ; \quad \xi = -[2(2s + 1) + 3b(s + 1)]/6, \quad (4)$$

where $s = 1 - 2\alpha$ and d is the component size. Thus, if we combine Equations 2, 3 and 4, and we can estimate the value of k_r , we can derive b and n , together with the spectral index α without further assumptions. Several studies (e.g., O’Sullivan & Gabuzda 2009; Sokolovsky et al 2011; Zdziarski et al. 2015) have shown that, in general, $k_r \sim 1$, as expected from equipartition arguments. Although this is not always the case for all sources (see e.g., Kadler et al 2004; Bach et al 2008; Kutkin et al 2014), Algaba et al. (2012) found $k_r = 0.9 \pm 0.1$ for 1633+382, which is consistent to the expected equipartition value. These considerations lead to the values of power-law indices $b = 1.5 \pm 0.2$ and $n = 1.1 \pm 0.2$, with a spectral index of $\alpha = -0.25 \pm 0.03$. These values are in agreement with the tentative ones discussed above.

If we consider simple flux density conservation without significant energy dissipation, poloidal magnetic fields scale as $B \propto R^{-2} \propto r^{-1.4}$, while toroidal fields scale as $B \propto R^{-1} \propto r^{-0.7}$, where we have used $R \propto r^{0.7}$. The value of $b = 1.5 \pm 0.2$ derived here thus suggest that poloidal magnetic fields are dominant in the jet. This implies that, under an assumption of a helical magnetic field distribution, the overall magnetic field in this region may maintain relatively larger pitch angle (e.g., $> 45^\circ$), or the emission region with larger pitch angle magnetic field (e.g., the spine structure, if a spine-sheath structure is considered) may dominate the radiation at radio wavelengths.

4.3. The Origin of the Jet Structure

Interestingly, the jet shows a significant bend within the first mas. Similarly, the components flux density seems to deviate from a pure power-law and to reach a local plateau within these distances (see Figure 2). It is possible that these two effects are related if the flux density plateau is produced by a change in the Doppler factor due to the jet bending. This bending may be caused by several different factors. One possibility could be interaction with the ambient medium. Indeed, in powerful FSRQs such as 1633+382, the presence of cold gas in the central regions is very likely, and not necessarily uniformly distributed. Within the Bondi radius, the central black hole should be having more influence and playing a much larger role, and ambient medium effects would potentially lead to the presence of pressure gradients which would translate into variations in the core shift offset $\Omega_{r,\nu}$ Lobanov (1998), which are not seen by investigating the values obtained from different frequency pairs based on the core shift for 1633+382 in Algaba et al. (2012). However, a significant amount of gas may be located downstream the jet. The jet bending could also result from the projection in the sky of a helical or

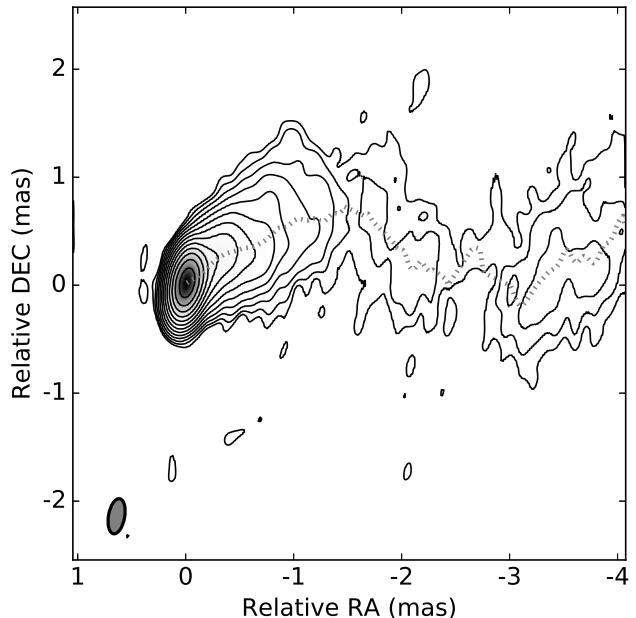


FIG. 7.— Stacked map of BU Blazar monitoring program for 1633+382. The root mean square of the map is rms=0.14 mJy. Contours start at $3 \times \text{rms}$ and increase in steps of 2. The grey oval in the bottom left of the map indicates the beam size. Dotted lines follow the ridge line of the jet.

harmonic jet trajectory, due to the presence of helical magnetic fields and/or of a binary SMBH.

In order to investigate these possibilities further, we stacked different epochs from the BU Blazar monitoring program from 2007 to 2016 weighted by their rms noise, so that we can increase the dynamic range for our analysis. We take into consideration two things here: i) the position angle PA of the jet seems to be slightly changing over time (see e.g., Ro et al. 2019), but the standard deviation of the PA for the epochs considered here is about 10° , which is acceptable for our purposes. ii) Periods of high flux densities which may affect the overall morphology of the source. In order to check this, we performed a similar analysis stacking only the images corresponding to a quiescent period. We checked that the results do not significantly differ.

The stacked map is shown in Figure 7. With the improved rms levels, details of the jet are revealed beyond 1 mas and its structure can be well followed up to 4 mas from the core. The bending of the jet, which was suggested by the component model-fitting is now clearly seen, and another possible bending is suggested at around 3 mas. This figure compares well with the corresponding MOJAVE⁴ images at 15 GHz, which clearly show the innermost jet bending, albeit the comparatively lower resolution, and the knot at 3-4 mas from the core. Overall, we find that the projection of the jet in the sky resembles that of a sinusoidal pattern.

We obtained the ridge line of the jet following Cohen et al. (2015). First, we made slices across the jet and fitted a gaussian to each profile. We considered both the peak of the fitted gaussian and the midpoint of the intensity across the jet as estimates for the ridge line. The points

⁴ <http://www.physics.purdue.edu/astro/MOJAVE>

were thereupon smoothed with a third-order spline. Both methods showed consistent results and followed well each other, deviating at most of the order of ~ 0.1 mas, which we will hereafter consider our uncertainty. The resulting ridge line is shown in Figure 7. The apparent sinusoidal pattern that the overall jet structure seems to follow is confirmed by the ridge line analysis.

We consider now the possible origin for this morphology. As mentioned above, one of the possibilities arises as the projection of a helical pattern. We follow Kun et al. (2014) to model the jet with a helical structure. Note that the conical helix they considered for 1928+738 is not appropriate for 1633+382, as we just found out that the jet geometry appears to be quasi-parabolic in the regions of our concern. Hence, the modified parametrization of the projected helical structure in the plane of the sky will become

$$\begin{aligned} x_{\text{jet}}^{\text{proj}} &= F(u) \cos(\lambda) - G(u) \sin(\lambda) \\ y_{\text{jet}}^{\text{proj}} &= F(u) \sin(\lambda) + G(u) \cos(\lambda) \end{aligned} \quad (5)$$

where

$$\begin{aligned} F(u) &= bu^\epsilon \cos(u - \phi) \cos \theta + au \sin \theta \\ G(u) &= bu^\epsilon \sin(u - \phi) \end{aligned} \quad (6)$$

with u the polar angle measured in the plane perpendicular to the jet axis, ϕ an initial phase, λ the P.A. rotation angle, $\epsilon = 0.71$ and $\theta = 2^\circ$. In Figure 8 we show the best model, which is found for $a = 21.0 \pm 0.5$, $b = 0.25 \pm 0.05$, $\phi = 6.0 \pm 0.2$ rad and $\lambda = 0.08 \pm 0.04$ rad. The model does not match well with several features of the ridge line: the first bend of the jet appears significantly sharper than expected by the model, and the trajectory downstream the jet seems not to follow the direction of the model. Furthermore, if the jet were to follow a helical pattern, this could produce a signature in the observed flux density due to Doppler boosting drifting as the viewing angle of the jet changes in its helical path. Although there is a flux density plateau which deviates from a single power law shown in Figure 2, this feature does not correlate with the ridge line pattern. Instead, the apparent kink at about 3.5 mas, for example, may be related with the properties of the observed jet knot at approximately that location.

Another appealing possibility is that the jet is precessing with time and the change of the position angle of the jet with distance is an indicator of such precession. Indeed, although we mentioned earlier that the innermost jet position angle does not change much during the period discussed here, Ro et al. (2019) suggests that, over much larger periods of time, there is a trend of the innermost jet position angle to change. If this is the case, we can estimate a possible precession period based on the sinusoidal pattern of the jet together with the jet speed. We consider a fit of the form

$$y_{\text{jet}}^{\text{proj}} = A \sin(Bx_{\text{jet}}^{\text{proj}} + C) + D, \quad (7)$$

which adjusts to the data with $B = 1.92 \pm 0.02$ mas. Combined with a speed of $140 \mu\text{as yr}^{-1}$ (see Paper II), this suggests a precession period of $T_{\text{obs}} \sim 23 \pm 5$ yr.

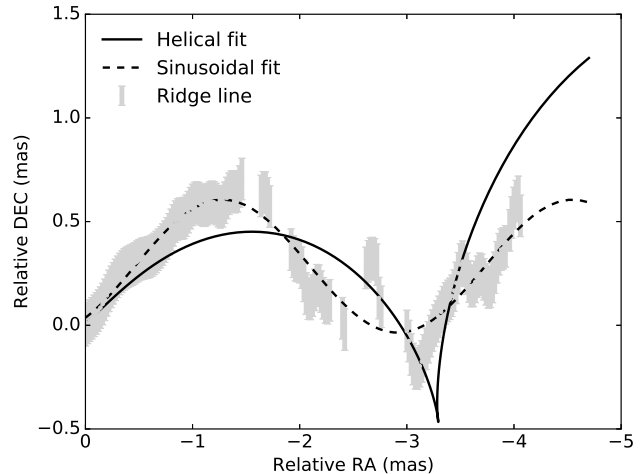


FIG. 8.— Models considered for fitting the jet ridge line of the stacked maps of 1633+382. Straight line: projection of a helical semi-parabolic pattern; dashed line: sinusoidal pattern.

Ro et al. (2019) also suggest that, if there is a periodic swinging of the jet, the period may be larger than ~ 20 years. The precession model, shown with a dashed line in Figure 8, also provides a better fitting for the data, with the ratio of χ^2 of the order of $\chi_{\text{helical}}^2 / \chi_{\text{sinusoidal}}^2 \sim 7$, although this alone is not sufficient to prefer any model. It is quite possible that the curving and wiggling of the jet results as a combination of different factors, including precession, helicity and instabilities or the growth of magneto-hydrodynamic instabilities. Some of such would include Kelvin-Helmholtz (see e.g. Perucho et al. 2006) or current-driven (see e.g. Meier & Nakamura 2006) instabilities. Other models where external causes, such as interaction with the surrounding medium, used to explain the wiggling, should also be considered.

5. CONCLUSIONS

In this paper we focus on the properties of the radio jet of 4C 38.41 (1633+382) and the evolution of the emerged components associated with the observed flux enhancement. For this purpose, we use high-resolution 43 GHz images from the BU-VLBA Monitoring program and study multi-epoch properties of the jet in terms of jet components. We consider the trajectory of the innermost regions of the jet, as well as its size and brightness temperature, and its relation with distance from the VLBI radio-core.

We find that the jet width follows a semi-parabolic geometry, with $R \propto r^{0.7}$, between the pure conical and the parabolic cases within regions considered to be upstream the jet, within mas scales. Additionally, there are hints suggesting the geometry downstream the jet may be conical, which indicates a possible collimation break at distances of the order of $10^6 r_g$, possibly within scales not too different from the estimated Bondi radius. This result is similar to that found in other sources, strengthening the suggestion that this may be a global characteristic of AGN jets.

Considering the brightness temperature profile and the geometry, together with core shift arguments, we can estimate the power-law dependences on the electron density and magnetic field strength to be in the form $N_e \propto r^{-1.1 \pm 0.2}$ and $B \propto r^{-1.5 \pm 0.2}$, respectively, for the

outmost components and the general trend. This suggests that the magnetic field is predominantly poloidal in the regions discussed here.

We analyse the structure of the innermost jet revealed by image staking. The innermost jet trajectory does not appear to be ballistic and, instead, matches well with a sinusoidal pattern. We consider various models from where the pattern arises, including a helical pattern or jet precession.

Acknowledgements. The authors are very grateful for a very fruitful discussion with M. Nakamura and H. Ro. This study makes use of 43 GHz VLBA data from the VLBA-BU Blazar Mon-

itoring Program (VLBA-BU-BLAZAR), funded by NASA through the *Fermi* Guest Investigator Program. The VLBA is an instrument of the National Radio Astronomy Observatory. The National Radio Astronomy Observatory is a facility of the National Science Foundation operated by Associated Universities, Inc. J. C. Algaba acknowledges support from the National Research Foundation of Korea (NRF) via grant NRF-2015R1D1A1A01056807 and support from Fundamental Research Grant Scheme (FRGS) FRGS/1/2019/STG02/UM/02/6. J. Park acknowledges support from the NRF via grant 2014H1A2A1018695. S. S. Lee was supported by the National Research Foundation of Korea (NRF) grant funded by the Korea government (MSIP) (No. NRF-2016R1C1B2006697). M. Kino acknowledges JSPS KAKENHI Grant Numbers JP18K03656 and JP18H03721. This research was supported by an appointment to the NASA Postdoctoral Program at the Goddard Space Flight Center, administered by Universities Space Research Association through a contract with NASA.

REFERENCES

- Abdo, A. A.; Ackermann, M.; Ajello, M.; et al. 2009, *ApJ*, 700, 597
- Acerro, F.; Ackermann, M.; Ajello, M.; et al. 2015 *ApJS* 218, 23
- Algaba, J. C.; Gabuzda, D. C.; Smith, P. S. 2012, *MNRAS* 420, 542
- Algaba, J. C.; Nakamura, M.; Asada, K.; et al. 2017 *ApJ* 834, 65
- Algaba, J. C.; Lee, S. S.; Kim, D. W., et al. 2018a *ApJ* 852, 30 (Paper I)
- Algaba, J. C.; Lee, S. S.; Rani, B., et al. 2018b *ApJ* 859, 128 (Paper II)
- Akiyama, K.; Asada, K.; Fish, V., et al. 2018 *Galax* 6, 15
- Aller, M. F., Aller, H. D., & Hughes, P. A. 1992, *ApJ*, 399, 16
- Asada, K.; Nakamura, M., 2012, *ApJ*, 745, 28
- Asada, K., Nakamura, M., Doi, A., Nagai, H., Inoue, M., 2014, *ApJ*, 781, 2
- Asada, K., Nakamura, M., Pu, H.-Y., 2016, *ApJ*, 833, 56
- Bach U., Krichbaum T. P., Middelberg E., et al. 2008, The 9th European VLBI Network Symp., The role of VLBI in the Golden Age for Radio Astronomy and EVN Users Meeting. *PoS*, p. 108
- Bednarek, W., & Kirk, J. G., 1995, *A&A* 294, 366
- Beuchert, T., Kadler, M., Perucho, M., et al. 2018, *A&A* 610, 32
- Blandford, R. D.; Znajek, R. L., 1977 *MNRAS*, 179, 433
- Cohen, M. H.; Meier, D. L.; Arshakian, T. G.; Clausen-Brown, E.; Homan, D. C.; Hovatta, T.; Kovalev, Y. Y.; Lister, M. L.; Pushkarev, A. B.; Richards, J. L.; Savolainen, T., 2015 *ApJ*, 803, 3
- Doelman, S. S.; Fish, V. L.; Schenck, D. E., et al., 2012 *Sci*, 338, 355
- Event Horizon Telescope Collaboration, Akiyama, K., Alberdi, A., et al. 2019, *ApJ*, 875, L1
- Ferrarese, L. & Merritt, D. 2000 *ApJ*, 539, 9
- Foreman-Mackey, D.; Hogg, D. W.; Lang, D., et al. 2013 *PASP* 125, 306
- Fomalont, E. B. 1999, *Synthesis Imaging in Radio Astronomy II*, 180, 301
- Gebhardt, K., Bender, R., Bower, G., et al., 2000 *ApJ* 539, L13
- Gómez, J. L., Gómez, J. L.; Lobanov, A. P.; Bruni, G., et al. 2016 *ApJ* 817, 96
- Hada, K.; Park, J. H., Kino, M. et al. 2017 *PASJ* 69, 71
- Hada, K.; Doi, A.; Wajima, K. et al. 2018 *ApJ* 860, 141
- Hewett, P. C.; Wild, V., 2010 *MNRAS* 405, 2302
- Homan, D. C.; Kovalev, Y. Y.; Lister, M. L.; et al. 2006, *ApJL*, 642, L115
- Hovatta, T.; Valtaoja, E.; Tornikoski, M.; et al. 2009, *A&A* 494, 527
- Jorstad, S. G.; Marscher, A. P.; Lister, M. L.; Stirling, A. M.; Cawthorne, T. V.; Gear, W. K.; Gmez, J. L.; Stevens, J. A.; Smith, P. S.; Forster, J. R.; Robson, E. I., 2005 *AJ*, 130, 1418
- Jorstad, S. G.; Marscher, A. P.; Agudo, I.; et al. 2011, *JApA* 32, 239
- Jorstad, S. G.; Marscher, A. P.; Morozova, D.A.; et al. 2017, *ApJ* 846, 98
- Kadler, M., Ros, E., Lobanov, A. P., Falcke, H., Zensus, J. A., 2004, *A&A* 426, 481
- Kardashev, N. S.; Novikov, I. D.; Lukash, V. N., et al. 2014 *PhyU*, 57, 1199
- Kino, M.; Takahara, F.; Kusunose, M. 2002 *ApJ* 564, 97
- Komissarov, S. S., Barkov, M. V.; Vlahakis, N.; Königl, A., 2007 *MNRAS* 380 51
- Komissarov, S. S., Vlahakis, N., Königl, A., & Barkov, M. V. 2009, *MNRAS*, 394, 1182
- Kovalev, Y. Y.; Kellermann, K. I.; Lister, M. L.; Homan, D. C.; Vermeulen, R. C.; Cohen, M. H.; Ros, E.; Kadler, M.; Lobanov, A. P.; Zensus, J. A.; Kardashev, N. S.; Gurvits, L. I.; Aller, M. F.; Aller, H. D., 2005 *AJ*, 130, 2473
- Kravchenko, E. V.; Kovalev, Y. Y.; Hovatta, T.; et al. 2016, *MNRAS* 462, 2747
- Kühr, H., Witzel, A., Pauliny-Toth, I. I. K., & Nauber, U. 1981, *A&AS*, 45, 367
- Kun, E.; Gabányi, K. É.; Karouzos, M., et al. 2014, *MNRAS* 445, 1370
- Kutkin, A. M.; Sokolovsky, K. V.; Lisakov, M. M.; et al. 2014 *MNRAS* 437,3396
- Lee, S. S.; Lobanov, A. P.; Krichbaum, T. P.; et al. 2008 *AJ*, 136, 159
- Lister, M. L.; Homan, D. C.; Hovatta, T.; et al. 2019 *ApJ*, 874, 43
- Liu, Y.; Jiang D. R.; Shen Z.-Q.; et al. 2010 *A&A* 522, A5
- Lobanov, A. P., 1998, *A&A*, 330, 79
- Lobanov, A. P. 2005, arXiv astro-ph/0503225
- Lu, R. S., Fish, V., Akiyama, K., 2013, *ApJ*, 772, 13
- Lyubarsky, Y. 2009, *ApJ*, 698, 1570
- McConnell, N. J., Ma, C. P., Gebhardt, K., et al. 2011 *Nature*, 480, 215
- Marscher, A. P. 1990, Parsec-scale radio jets, Proceedings of a workshop, held at National Radio Astronomy Observatory, Socorro, New Mexico, October 17-18, 1989. Edited by J. Anton Zensus and Timothy J. Pearson. Cambridge: Cambridge University Press., p.236
- Meier, D. L., & Nakamura, M. 2006, *ASP Conf. Ser.*, 350
- Merritt, D. & Ferrarese, L., 2001, *ApJ* 547, 140
- Murphy, D. W.; Browne, I. W. A.; Perley, R. A. 1993, *MNRAS*, 264, 298
- Nakahara, S.; Doi, A.; Murata, Y.; et al. 2018, *ApJ* 854, 148
- Nokhrina E. E., 2017, *MNRAS*, 468, 2372
- O'Sullivan, S. P. & Gabuzda, D. C. 2009, *MNRAS*, 400, 26
- Perucho, M., Lobanov, A. P., Martí, J. M., & Hardee, P. E. 2006, *A&A*, 456, 493
- Pilipenko, S. V.; Kovalev, Y. Y.; Andrianov, A. S., et al. 2018, *MNRAS* 474, 3523
- Pushkarev, A. B.; Hovatta, T.; Kovalev, Y. Y.; Lister, M. L.; Lobanov, A. P.; Savolainen, T.; Zensus, J. A., 2012, *A&A*, 545, 113
- Pushkarev, A. B.; Kovalev, Y. Y.; Lister, M.; et al. 2017 *MNRAS* 468, 4992
- Raiteri, C. M.; Villata, M.; Smith, P. S.; et al. 2012, *A&A* 545, 48
- Ro, H., Sohn, W.-B., et al. *PoS*, proceedings for the 14th European VLBI Network Symposium & Users Meeting, 8-11 October. Granada, Spain. Eds I. Agudo, J. Conway, and A. Alberdi
- Seielstad, G. A., Pearson, T. J., & Readhead, A. C. S. 1985, *PASP*, 95, 842
- Shepherd, M. C. 1997, in *ASP Conf. Ser. 125, Astronomical Data Analysis Software and Systems VI*, ed. G. Hunt & H. E. Payne (San Francisco, CA: ASP), 77
- Sokolovsky, K. V., Kovalev, Y. Y., Pushkarev, A. B., et al. 2011, *A&A*, 532, A38
- Spangler, S. R., & Cotton, W. D. 1981, *AJ*, 86, 730
- Tchekhovskoy, A., McKinney, J. C., & Narayan, R. 2008, *MNRAS*, 388, 551
- Tsang, C.-Y.; Asada, K.; Nakamura, M.; et al. 2006, *ApJ*, 833, 288
- Zamaninasab, M., Clausen-Brown, E., Savolainen, T., et al. 2014, *Nature* 510, 126
- Zdziarski A. A., Sikora M., Pjanka P., Tchekhovskoy A., 2015, *MNRAS*, 451, 927